Journal of Geophysical Research: Solid Earth

Supporting Information for

Thermal nature of mantle upwellings below the Ibero-western Maghreb region inferred from teleseismic tomography

Chiara Civiero[1,2], Susana Custódio[1], Nicholas Rawlinson[3], Vincent Strak[4], Graça Silveira[1,5], Pierre Arroucau[6], Carlos Corela[1]

[1]Instituto Dom Luiz (IDL), Faculdade de Ciências, Universidade de Lisboa, Lisboa 1749-016, Portugal

[2] Dublin Institute for Advanced Studies (DIAS), Dublin D02 Y006, Ireland

[3] Bullard Laboratories, Department of Earth Sciences, University of Cambridge, Cambridge CB30EZ, UK

[4] Department of Earth Sciences, Vrije Universiteit Amsterdam, Amsterdam 1081 HV, Netherlands

[5] Instituto Superior de Engenharia de Lisboa, Lisboa 1959-007, Portugal

[6]EDF/DIPNN/DI/TEGG/SGG, Groupe Aléa Sismique, Aix-en-Provence, France

Contents of this file

Introduction

The supporting information contains additional figures to further illustrate:
- some steps of the data processing such as the analysis of the relative arrival-time residuals (Figure S1) and the trade-off curve to decide the best smoothing and damping parameters for our inversion (Figure S3)
- the *3D* starting model used in the inversion to generate our preferred *S*-wave model (Figure S2)
- an additional checkerboard resolution test using bigger synthetic anomalies (Figure S4)
- slices and cross-sections from our previously published *P*-wave model, IBEM-P18, (Civiero et al., 2018) to facilitate the comparison with the *S*-wave model (Figures S5 and S6)
- the resulting inversions using different starting models (i.e., *ak135* and *SeMum2* models) which contain the same first-order characteristics of our preferred model (Figures S7 and S8).
- a structural resolution test for previous *P*-wave dataset to compute the amplitude recovery for scaling the velocity and temperature anomalies (Figure S9).
- two V-T conversion in the three regions *A1*, *A2* and *A3* using different maximum velocity perturbations in the input structures: -0.1 km/s (Figure S10) and -0.6 km/s (Figure S11).

In addition, the supplementary tables contain (i) the details of all the stations, networks and project from which data were used in this study (Table S1): (ii) the P- and S-wave arrival-time residuals for each region *A1, A2* and *A3* needed to build Figure 6 (Table S2).

Station	*Net*	*Lat (º)*	*Long (º)*	*Elev (km)*	*Project/Institution*
AGUA	YF	36.94	-1.92	-0.15	Midsea Temporary Network
ALHU	IB	35.21	-3.89	-0.06	IberArray
ALJ	IB	36.53	-5.65	-0.48	IberArray
AVE	WM	33.30	-7.41	-0.23	Western Mediterranean Seismic Network
CADI	CA	42.34	1.84	-1.21	Catalan Seismic Network
CART	GE	37.59	-1.00	-0.07	Geofon
CBRU	CA	42.29	2.18	-1.33	Catalan Seismic Network
CCUM	ES	27.75	-18.03	-0.46	Spanish Digital Seismic Network
CDLU	YF	36.93	-2.30	-0.40	Midsea Temporary Network
CEU	GE	35.90	-5.37	-0.32	Geofon
CFUE	ES	28.65	-13.94	-0.18	Spanish Digital Seismic Network
CHAF	IB	35.18	-2.43	-0.09	IberArray
CJUL	ES	27.73	-18.08	-1.28	Spanish Digital Seismic Network
COBS	CA	40.71	1.36	0.00	Catalan Seismic Network
COI	SS	40.21	-8.41	-0.14	Centro de Geofisica da Universidade de Coimbra
CRAJ	ES	28.26	-16.60	-2.47	Spanish Digital Seismic Network
CSOR	CA	42.38	1.13	-1.23	Catalan Seismic Network
CTAB	ES	27.75	-18.09	-0.15	Spanish Digital Seismic Network
CTAN	ES	27.75	-18.05	-0.02	Spanish Digital Seismic Network
CTIG	ES	27.79	-17.92	-0.53	Spanish Digital Seismic Network
CTRE	CA	42.32	0.77	-1.32	Catalan Seismic Network
E001	IB	36.17	-5.84	-0.35	IberArray
E006	IB	36.95	-5.04	-1.03	IberArray
E007	IB	36.86	-3.43	-1.29	IberArray
E008	IB	37.50	-7.13	-0.18	IberArray
E009	IB	37.42	-6.77	-0.15	IberArray
E010	IB	36.99	-6.44	-0.05	IberArray
E011	IB	37.21	-5.99	-0.06	IberArray
E012	IB	37.37	-5.52	-0.14	IberArray
E013	IB	36.96	-4.53	-1.22	IberArray
E015	IB	37.17	-3.11	-1.32	IberArray
E016	IB	37.97	-7.06	-0.32	IberArray
E017	IB	37.57	-6.23	-0.26	IberArray

E018	IB	37.98	-5.95	-0.39	IberArray
E019	IB	37.72	-5.88	-0.12	IberArray
E020	IB	37.57	-4.84	-0.31	IberArray
E021	IB	38.01	-4.92	-0.61	IberArray
E022	IB	37.90	-4.38	-0.39	IberArray
E024	IB	37.72	-3.92	-1.24	IberArray
E025	IB	37.70	-3.47	-1.62	IberArray
E026	IB	37.50	-2.59	-1.09	IberArray
E028	IB	38.36	-6.81	-0.60	IberArray
E029	IB	38.44	-6.18	-0.59	IberArray
E030	IB	38.47	-5.63	-0.63	IberArray
E031	IB	38.34	-5.00	-0.69	IberArray
E032	IB	38.11	-3.49	-0.48	IberArray
E033	IB	38.36	-2.91	-0.69	IberArray
E034	IB	38.23	-2.19	-1.29	IberArray
E035	IB	37.99	-0.94	-0.30	IberArray
E036	IB	38.85	-6.44	-0.32	IberArray
E037	IB	38.89	-5.88	-0.44	IberArray
E038	IB	38.73	-5.24	-0.60	IberArray
E039	IB	38.82	-4.69	-0.59	IberArray
E040	IB	36.61	-4.20	-0.75	IberArray
E041	IB	38.65	-3.66	-0.83	IberArray
E042	IB	38.81	-3.02	-0.89	IberArray
E044	IB	38.86	-2.07	-0.81	IberArray
E045	IB	38.78	-0.86	-0.70	IberArray
E046	IB	39.29	-6.67	-0.35	IberArray
E047	IB	39.28	-6.19	-0.54	IberArray
E048	IB	39.31	-5.50	-0.50	IberArray
E049	IB	39.17	-4.83	-0.73	IberArray
E050	IB	39.10	-4.13	-0.79	IberArray
E051	IB	38.99	-3.67	-0.69	IberArray
E052	IB	39.28	-3.10	-0.70	IberArray
E053	IB	39.19	-2.59	-0.83	IberArray
E054	IB	39.38	-2.05	-0.82	IberArray
E055	IB	39.18	-1.38	-0.73	IberArray

E056	IB	39.13	-0.64	-0.23	IberArray
E057	IB	39.75	-6.59	-0.37	IberArray
E058	IB	39.82	-5.92	-0.35	IberArray
E059	IB	39.74	-5.15	-0.53	IberArray
E060	IB	39.76	-4.63	-0.63	IberArray
E061	IB	39.66	-3.27	-0.72	IberArray
E062	IB	39.64	-2.53	-0.87	IberArray
E063	IB	39.95	-2.08	-1.18	IberArray
E064	IB	39.66	-1.46	-0.94	IberArray
E066	IB	39.87	-0.43	-0.46	IberArray
E067	IB	40.23	-6.86	-0.61	IberArray
E068	IB	40.23	-6.21	-0.44	IberArray
E069	IB	40.14	-5.45	-0.63	IberArray
E070	IB	40.22	-4.80	-0.49	IberArray
E071	IB	40.28	-4.19	-0.59	IberArray
E072	IB	40.07	-3.52	-0.56	IberArray
E073	IB	40.14	-2.91	-0.81	IberArray
E074	IB	40.13	-2.42	-1.08	IberArray
E075	IB	40.23	-1.57	-1.49	IberArray
E076	IB	40.14	-1.06	-1.85	IberArray
E077	IB	40.26	0.10	-0.41	IberArray
E078	IB	40.67	-6.48	-0.91	IberArray
E079	IB	40.65	-5.87	-1.01	IberArray
E080	IB	40.60	-5.13	-1.43	IberArray
E081	IB	40.61	-4.42	-1.36	IberArray
E082	IB	40.53	-3.80	-0.74	IberArray
E083	IB	40.52	-3.29	-0.59	IberArray
E084	IB	40.58	-2.65	-1.04	IberArray
E085	IB	40.50	-1.97	-1.54	IberArray
E086	IB	40.56	-1.10	-1.28	IberArray
E087	IB	40.68	-0.32	-0.94	IberArray
E088	IB	41.13	-6.13	-0.81	IberArray
E089	IB	41.11	-5.38	-0.84	IberArray
E090	IB	41.07	-4.79	-0.92	IberArray
E091	IB	41.09	-4.09	-0.98	IberArray

E092	IB	41.07	-3.46	-1.37	IberArray
E093	IB	40.98	-2.76	-1.02	IberArray
E094	IB	40.96	-1.44	-1.12	IberArray
E095	IB	41.04	-0.85	-0.87	IberArray
E096	IB	41.05	0.87	-0.28	IberArray
E097	IB	41.56	-5.80	-0.76	IberArray
E098	IB	41.59	-5.09	-0.88	IberArray
E099	IB	41.54	-4.46	-0.93	IberArray
E100	IB	41.50	-3.76	-1.08	IberArray
E101	IB	41.45	-2.97	-1.05	IberArray
E102	IB	41.30	-2.36	-1.01	IberArray
E103	IB	41.25	-1.70	-0.75	IberArray
E104	IB	41.38	-1.08	-0.66	IberArray
E105	IB	41.19	-0.38	-0.35	IberArray
E106	IB	41.31	0.43	-0.52	IberArray
E107	IB	41.33	1.46	-0.68	IberArray
E109	IB	42.12	-7.35	-1.15	IberArray
E110	IB	41.99	-6.13	-0.82	IberArray
E111	IB	42.03	-5.48	-0.80	IberArray
E112	IB	41.99	-4.73	-0.81	IberArray
E113	IB	41.92	-4.09	-0.98	IberArray
E114	IB	41.92	-3.37	-1.19	IberArray
E115	IB	41.80	-2.62	-1.11	IberArray
E116	IB	41.77	-2.01	-1.20	IberArray
E117	IB	41.75	-1.40	-0.43	IberArray
E118	IB	42.01	-0.95	-0.79	IberArray
E119	IB	41.84	0.24	-0.47	IberArray
E120	IB	41.72	1.11	-0.37	IberArray
E121	IB	41.67	1.99	-0.98	IberArray
E122	IB	42.36	-8.04	-0.47	IberArray
E123	IB	42.40	-6.95	-0.86	IberArray
E124	IB	42.48	-6.49	-1.17	IberArray
E125	IB	42.45	-5.69	-0.92	IberArray
E126	IB	42.43	-5.06	-0.90	IberArray
E127	IB	42.48	-4.36	-0.93	IberArray

E128	IB	42.41	-3.65	-1.02	IberArray
E129	IB	42.31	-2.85	-0.94	IberArray
E130	IB	42.26	-2.27	-1.04	IberArray
E131	IB	42.19	-1.53	-0.33	IberArray
E132	IB	42.38	-0.96	-0.98	IberArray
E133	IB	42.20	-0.34	-0.72	IberArray
E134	IB	42.25	0.14	-1.13	IberArray
E135	IB	42.20	1.82	-1.17	IberArray
E136	IB	42.06	2.50	-1.08	IberArray
E137	IB	42.63	-8.48	-0.43	IberArray
E138	IB	42.85	-7.97	-0.40	IberArray
E139	IB	42.94	-7.51	-0.46	IberArray
E140	IB	42.95	-6.87	-0.64	IberArray
E141	IB	42.82	-6.05	-1.23	IberArray
E142	IB	42.89	-5.42	-1.41	IberArray
E143	IB	42.91	-4.61	-1.27	IberArray
E144	IB	42.89	-3.88	-0.89	IberArray
E145	IB	42.80	-3.21	-0.64	IberArray
E146	IB	42.76	-2.63	-0.89	IberArray
E147	IB	42.79	-2.01	-1.16	IberArray
E148	IB	42.81	-1.02	-0.96	IberArray
E150	IB	43.15	-8.50	-0.40	IberArray
E151	IB	43.31	-7.87	-0.55	IberArray
E152	IB	43.27	-6.38	-0.38	IberArray
E153	IB	43.23	-5.72	-0.89	IberArray
E154	IB	43.35	-4.60	-0.41	IberArray
E155	IB	43.24	-4.00	-0.68	IberArray
E156	IB	43.14	-2.76	-0.31	IberArray
E157	IB	43.17	-2.13	-0.69	IberArray
E158	IB	42.66	0.19	-1.45	IberArray
E908	IB	42.09	-8.74	-0.14	IberArray
E920	IB	41.73	1.28	-0.52	IberArray
E932	IB	38.15	-3.47	-0.42	IberArray
E961	IB	39.66	-3.33	-0.74	IberArray
E992	IB	41.08	-3.55	-1.34	IberArray

E994	IB	40.96	-1.40	-1.11	IberArray
EBAJ	ES	28.54	-16.34	-0.24	Spanish Digital Seismic Network
EBR	EB	40.82	0.49	-0.04	Ebre Observatory Regional Seismic Network
ECAL	ES	41.94	-6.74	-0.95	Spanish Digital Seismic Network
ECHE	IB	39.59	-0.97	-0.70	IberArray
EFAM	ES	29.13	-13.53	-0.14	Spanish Digital Seismic Network
EGOM	ES	28.16	-17.21	-0.78	Spanish Digital Seismic Network
EHIG	ES	28.56	-17.81	-0.84	Spanish Digital Seismic Network
EHUE	IB	37.81	-2.59	-1.03	IberArray
EJON	ES	42.45	2.89	-0.57	Spanish Digital Seismic Network
ELOJ	IB	37.15	-4.15	-1.04	IberArray
ELUQ	IB	37.56	-4.27	-0.75	IberArray
EMUR	ES	37.84	-1.24	-0.57	Spanish Digital Seismic Network
EOSO	ES	28.07	-15.55	-0.76	Spanish Digital Seismic Network
ES01	YF	37.03	-1.93	0.00	Midsea Temporary Network
ES02	YF	37.03	-1.93	-0.10	Midsea Temporary Network
ES03	YF	37.03	-1.93	-0.07	Midsea Temporary Network
ES04	YF	37.03	-1.92	-0.10	Midsea Temporary Network
ES05	YF	37.02	-1.92	-0.07	Midsea Temporary Network
EVIA	IB	38.67	-2.50	-1.17	IberArray
EVO	WM	38.53	-8.01	-0.23	Western Mediterranean Seismic Network
EZAM	IB	42.15	-8.70	-0.46	IberArray
FBR	CA	41.42	2.12	-0.41	Catalan Seismic Network
FINC	YF	37.10	-1.96	-0.40	Midsea Temporary Network
GGNV	LX	38.72	-9.15	-0.08	University of Lisbon
HORN	YF	36.89	-2.08	-0.25	Midsea Temporary Network
LIJA	IB	36.91	-5.40	-1.00	IberArray
LPNR	YF	37.17	-1.98	-0.45	Midsea Temporary Network
LRDN	YF	37.05	-2.01	-0.46	Midsea Temporary Network
LUBR	YF	37.21	-2.07	-0.60	Midsea Temporary Network
LUCA	YF	37.04	-2.18	-0.51	Midsea Temporary Network
M001	IB	33.93	-6.76	-0.19	IberArray
M002	IB	35.37	-5.97	-0.24	IberArray
M004	IB	34.79	-6.25	-0.12	IberArray
M005	IB	35.02	-5.40	-0.20	IberArray

M006	IB	34.94	-4.78	-1.05	IberArray
M007	IB	34.76	-3.80	-1.34	IberArray
M008	IB	34.73	-2.80	-0.30	IberArray
M010	IB	34.21	-6.34	-0.12	IberArray
M011	IB	34.02	-5.47	-0.84	IberArray
M012	IB	34.73	-5.43	-0.23	IberArray
M013	IB	34.61	-4.41	-0.54	IberArray
M014	IB	33.94	-3.84	-0.92	IberArray
M015	IB	33.98	-3.04	-1.08	IberArray
M016	IB	34.38	-2.16	-1.61	IberArray
M017	IB	33.70	-5.99	-0.66	IberArray
M018	IB	33.62	-4.45	-1.09	IberArray
M019	IB	31.94	-4.46	-1.09	IberArray
M201	IB	33.27	-6.17	-0.86	IberArray
M202	IB	32.92	-5.51	-1.44	IberArray
M203	IB	32.15	-5.63	-2.22	IberArray
M204	IB	30.86	-9.05	-0.95	IberArray
M205	IB	32.38	-6.32	-0.61	IberArray
M206	IB	32.80	-6.58	-0.75	IberArray
M207	IB	31.19	-8.06	-1.06	IberArray
M208	IB	29.58	-10.03	-0.12	IberArray
M210	IB	32.35	-4.08	-1.43	IberArray
M211	IB	30.92	-7.25	-1.39	IberArray
M212	IB	33.36	-6.67	-0.73	IberArray
M213	IB	32.21	-8.55	-0.38	IberArray
M214	IB	31.82	-6.68	-1.25	IberArray
M215	IB	32.05	-7.45	-0.52	IberArray
M216	IB	34.84	-3.41	-0.54	IberArray
M217	IB	31.55	-5.55	-1.40	IberArray
M218	IB	31.55	-5.55	-1.40	IberArray
M301	IB	32.47	-7.86	-0.56	IberArray
M310	IB	31.24	-6.09	-1.49	IberArray
M316	IB	31.80	-8.64	-0.31	IberArray
MAHO	GE	39.90	4.27	-0.01	Geofon
MELI	GE	35.29	-2.94	-0.01	Geofon

MESJ	LX	37.84	-8.22	-0.25	University of Lisbon
MM01	3D	31.54	-7.68	-0.77	University of Munster
MM02	3D	31.23	-7.42	-2.00	University of Munster
MM03	3D	30.88	-6.90	-1.20	University of Munster
MM04	3D	30.74	-6.63	-1.53	University of Munster
MM05	3D	30.68	-6.39	-0.99	University of Munster
MM06	3D	30.51	-6.07	-0.87	University of Munster
MM07	3D	30.26	-5.61	-0.73	University of Munster
MM08	3D	31.03	-6.49	-1.28	University of Munster
MM09	3D	30.59	-7.20	-1.47	University of Munster
MM10	3D	30.53	-7.93	-1.06	University of Munster
MM11	3D	30.65	-8.60	-0.57	University of Munster
MM12	3D	30.41	-8.83	-0.34	University of Munster
MM13	3D	30.54	-9.58	-0.42	University of Munster
MM14	3D	30.04	-9.17	-0.77	University of Munster
MM15	3D	31.20	-8.90	-0.95	University of Munster
MORF	LX	37.30	-8.65	-0.56	University of Lisbon
MTE	GE	40.40	-7.54	-0.81	Geofon
MTLF	RD	43.34	2.22	-0.36	Resif
MTOR	IP	28.49	-9.85	-0.32	Instituto Superior Tecnico Broadband Seismic Network
MTT2	RD	43.34	2.22	-0.36	Resif
NKM	IB	35.45	-5.41	-0.42	IberArray
OBS04	NT	36.95	-9.70	1.99	NEAREST
OBS10	NT	36.25	-8.60	2.07	NEAREST
OBS12	NT	36.08	-10.59	4.86	NEAREST
OBS14	NT	36.00	-9.40	2.44	NEAREST
OBS16	NT	35.95	-8.25	2.07	NEAREST
OBS18	NT	35.71	-10.34	4.61	NEAREST
OBS19	NT	35.63	-9.75	4.29	NEAREST
OBS20	NT	35.60	-9.10	3.45	NEAREST
OBS21	NT	35.65	-8.60	2.57	NEAREST
OBS25	NT	36.36	-9.57	3.23	NEAREST
PACT	IP	38.77	-8.83	-0.03	Instituto Superior Tecnico Broadband Seismic Network

PBAR	PM	38.17	-7.04	-0.20	Portuguese National Seismic Network
PESTR	PM	38.87	-7.59	-0.41	Portuguese National Seismic Network
PFVI	PM	37.13	-8.83	-0.19	Portuguese National Seismic Network
PM01	XB	35.70	-5.65	-0.28	PICASSO
PM02	XB	35.61	-5.35	-0.17	PICASSO
PM03	XB	35.51	-5.77	-0.13	PICASSO
PM04	XB	35.40	-5.15	-0.11	PICASSO
PM05	XB	35.21	-5.34	-0.51	PICASSO
PM06	XB	35.31	-5.64	-0.26	PICASSO
PM07	XB	35.23	-4.99	-0.71	PICASSO
PM08	XB	35.14	-4.71	-0.25	PICASSO
PM09	XB	35.03	-5.11	-0.52	PICASSO
PM10	XB	34.74	-5.14	-0.28	PICASSO
PM11	XB	34.93	-4.31	-1.00	PICASSO
PM12	XB	34.85	-4.61	-1.59	PICASSO
PM13	XB	34.67	-4.94	-0.58	PICASSO
PM14	XB	34.55	-5.13	-0.27	PICASSO
PM15	XB	34.47	-4.70	-0.42	PICASSO
PM16	XB	35.13	-3.69	-0.66	PICASSO
PM17	XB	34.39	-5.30	-0.36	PICASSO
PM18	XB	34.15	-4.82	-0.46	PICASSO
PM19	XB	34.14	-5.13	-0.34	PICASSO
PM20	XB	33.91	-5.03	-0.68	PICASSO
PM21	XB	33.72	-5.32	-1.01	PICASSO
PM22	XB	33.29	-5.11	-1.95	PICASSO
PM22B	XB	33.31	-5.10	-1.92	PICASSO
PM23	XB	33.13	-5.03	-1.99	PICASSO
PM24	XB	33.00	-4.90	-1.60	PICASSO
PM25	XB	32.88	-4.89	-1.42	PICASSO
PM26	XB	32.52	-4.57	-1.84	PICASSO
PM27	XB	32.35	-4.65	-1.47	PICASSO
PM28	XB	32.23	-4.62	-1.40	PICASSO
PM29	XB	32.08	-4.39	-1.23	PICASSO
PM30	XB	31.86	-4.27	-1.02	PICASSO
PM31	XB	32.71	-4.72	-1.51	PICASSO

PM31A	XB	32.72	-4.74	-1.42	PICASSO
PM32	XB	31.57	-4.19	-0.90	PICASSO
PM33	XB	31.43	-4.24	-0.85	PICASSO
PM33A	XB	31.41	-4.29	-0.85	PICASSO
PM34	XB	31.29	-4.11	-0.81	PICASSO
PM35	XB	31.05	-4.00	-0.74	PICASSO
PM36	XB	34.89	-3.74	-0.78	PICASSO
PM37	XB	34.95	-3.15	-0.28	PICASSO
PM38	XB	34.84	-2.87	-0.46	PICASSO
PM39	XB	34.89	-2.61	-0.21	PICASSO
PM40	XB	34.91	-2.21	-0.39	PICASSO
PMOZ	PM	32.79	-17.11	-1.03	Portuguese National Seismic Network
PMST	IP	38.74	-9.18	-0.17	Instituto Superior Tecnico Broadband Seismic Network
POBL	CA	41.38	1.08	-0.55	Catalan Seismic Network
POLO	PM	41.37	-7.79	-1.06	Portuguese National Seismic Network
PS01	XB	36.08	-5.62	-0.08	PICASSO
PS02	XB	36.26	-5.37	-0.20	PICASSO
PS03	XB	36.39	-5.42	-0.13	PICASSO
PS04	XB	36.61	-5.32	-0.46	PICASSO
PS05	XB	36.65	-5.09	-1.15	PICASSO
PS06	XB	36.73	-5.51	-0.34	PICASSO
PS07	XB	36.67	-4.80	-0.25	PICASSO
PS08	XB	36.74	-4.64	-0.16	PICASSO
PS09	XB	36.82	-5.23	-0.92	PICASSO
PS10	XB	36.80	-4.90	-0.64	PICASSO
PS11	XB	36.87	-4.68	-0.28	PICASSO
PS12	XB	37.05	-5.19	-0.55	PICASSO
PS13	XB	37.06	-4.75	-0.48	PICASSO
PS14	XB	37.15	-5.52	-0.20	PICASSO
PS15	XB	37.14	-4.50	-0.67	PICASSO
PS16	XB	37.21	-5.05	-0.37	PICASSO
PS17	XB	37.29	-5.39	-0.23	PICASSO
PS18	XB	37.25	-4.74	-0.49	PICASSO
PS19	XB	37.37	-4.99	-0.25	PICASSO

PS21	XB	37.34	-4.46	-0.55	PICASSO
PS22	XB	37.37	-4.70	-0.36	PICASSO
PS23	XB	37.56	-5.10	-0.26	PICASSO
PS24	XB	37.61	-5.40	-0.18	PICASSO
PS26	XB	37.72	-4.96	-0.25	PICASSO
PS30	XB	37.84	-4.90	-0.15	PICASSO
PS33	XB	38.16	-4.91	-0.75	PICASSO
PS34	XB	38.43	-4.75	-0.68	PICASSO
PS35	XB	38.71	-4.88	-0.47	PICASSO
PS37	XB	39.00	-4.96	-0.58	PICASSO
PS39	XB	39.39	-5.00	-0.56	PICASSO
PS40	XB	39.49	-4.84	-0.67	PICASSO
PS41	XB	36.67	-5.94	-0.13	PICASSO
PS42	XB	36.53	-5.04	-0.23	PICASSO
PS44	XB	36.32	-5.99	-0.10	PICASSO
PS45	XB	36.31	-5.72	-0.12	PICASSO
PS46	XB	36.82	-4.34	-0.66	PICASSO
PS47	XB	36.87	-4.08	-0.66	PICASSO
PS48	XB	36.90	-3.73	-1.34	PICASSO
PS49	XB	36.90	-3.18	-1.22	PICASSO
PS51	XB	36.97	-4.89	-0.44	PICASSO
PS52	XB	37.00	-4.23	-1.08	PICASSO
PS53	XB	37.06	-3.96	-0.96	PICASSO
PS56	XB	37.11	-3.44	-1.94	PICASSO
PS57	XB	37.01	-2.99	-1.29	PICASSO
PS58	XB	37.26	-4.00	-0.84	PICASSO
PS59	XB	37.32	-3.80	-0.81	PICASSO
PS60	XB	37.33	-3.45	-1.55	PICASSO
PS61	XB	37.29	-3.07	-1.19	PICASSO
PVAQ	PM	37.40	-7.72	-0.20	Portuguese National Seismic Network
PW01	8A	41.67	-8.79	-0.10	WILAS
PW02	8A	41.45	-8.46	-0.16	WILAS
PW03	8A	41.69	-7.50	-0.53	WILAS
PW04	8A	41.55	-7.18	-0.25	WILAS
PW05	8A	41.42	-6.48	-0.65	WILAS

PW06	8A	41.00	-8.27	-0.35	WILAS
PW07	8A	40.94	-7.50	-0.90	WILAS
PW08	8A	40.66	-6.99	-0.75	WILAS
PW09	8A	40.67	-8.53	-0.08	WILAS
PW11	8A	40.57	-8.18	-0.79	WILAS
PW12	8A	40.20	-8.86	-0.44	WILAS
PW13	8A	39.77	-8.92	-0.08	WILAS
PW14	8A	39.62	-8.41	-0.10	WILAS
PW15	8A	39.84	-7.48	-0.39	WILAS
PW16	8A	39.77	-7.07	-0.30	WILAS
PW17	8A	39.35	-9.29	-0.10	WILAS
PW18	8A	39.46	-7.89	-0.23	WILAS
PW19	8A	38.85	-8.50	-0.11	WILAS
PW20	8A	38.53	-8.36	-0.27	WILAS
PW22	8A	39.51	-8.80	-0.51	WILAS
REAL	IB	36.49	-5.21	-1.49	IberArray
RODA	YF	36.84	-2.05	-0.14	Midsea Temporary Network
RTC	MN	33.99	-6.86	-0.05	MedNet
SFS	GE	36.47	-6.21	-0.02	Geofon
SN02	YF	37.06	-1.88	-0.18	Midsea Temporary Network
SN03	YF	37.06	-1.88	-0.20	Midsea Temporary Network
SN04	YF	37.06	-1.88	-0.20	Midsea Temporary Network
SN05	YF	37.06	-1.88	-0.19	Midsea Temporary Network
ST01	YF	37.05	-1.88	-0.11	Midsea Temporary Network
ST02	YF	37.05	-1.88	-0.10	Midsea Temporary Network
ST03	YF	37.05	-1.88	-0.11	Midsea Temporary Network
ST04	YF	37.05	-1.88	-0.11	Midsea Temporary Network
STEO	WM	37.55	-8.72	0.00	Western Mediterranean Seismic Network
TAF	IB	34.81	-2.41	-0.85	IberArray
URRA	YF	37.10	-2.10	-0.38	Midsea Temporary Network

Table S1. Seismic stations (Sta = station code, Net = network code, Lat = latitude, Long = longitude and El = elevation) used in the tomographic study and the corresponding names of the project or institution involved. DOIs (when available) are: https://doi.org/10.7914/SN/CA for the Catalan Seismic Network, doi:10.14470/TR560404 for Geofon, https://doi.org/10.13127/sd/fbbbtdtd6q for MedNet, https://doi.org/10.14470/JZ581150 for the Western Mediterranean Seismic Network, https://doi.org/10.7914/SN/XB_2009 for PICASSO,

https://doi.org/10.7914/SN/IB for IberArray, https://doi.org/10.7914/SN/3D_2010 for stations from the University of Munster, https://doi.org/10.14470/3N7565750319 for WILAS.

P-wave residuals	*S-wave residuals*	*error on P*	*error on S*
A1			
-0.15	-1.10	0.15	0.46
0.40	0.65	0.15	0.39
-0.05	0.15	0.15	0.75
-0.35	-0.65	0.09	0.15
0.25	-1.10	0.15	0.46
1.00	1.50	0.15	0.75
0.70	0.70	0.15	0.75
0.10	0.05	0.15	0.75
-1.05	-2.00	0.15	0.43
-0.50	-0.75	0.15	0.59
-1.40	-1.75	0.15	0.75
-1.10	-2.00	0.15	0.74
-0.60	-1.60	0.15	0.75
-0.10	-2.00	0.15	0.44
0.25	-2.60	0.15	0.75
-0.05	-3.35	0.15	0.75
0.25	-1.15	0.15	0.75
0.05	-0.25	0.15	0.75
0.30	2.50	0.15	0.75
-0.45	-0.20	0.15	0.75
-0.05	-2.45	0.15	0.75
0.90	1.85	0.14	0.75
0.05	-2.15	0.15	0.68
-0.30	-3.00	0.15	0.55
-0.10	-2.70	0.15	0.75
0.25	-1.75	0.15	0.60
-0.35	-2.05	0.15	0.75
0.35	-0.90	0.15	0.75
0.75	0.55	0.15	0.68
0.15	0.50	0.15	0.75
-0.25	-1.15	0.15	0.75
-0.20	-2.20	0.15	0.75
0.45	-1.25	0.15	0.75
0.05	-0.35	0.15	0.75
-0.05	-1.35	0.15	0.75
0.20	-0.15	0.15	0.64
0.65	-0.60	0.15	0.68
0.25	-0.05	0.15	0.75
0.55	-0.85	0.15	0.75
0.20	-3.70	0.15	0.75
0.30	-1.05	0.15	0.75

1.20	2.45	0.15	0.75
0.70	0.15	0.15	0.55
1.15	2.90	0.15	0.75
0.80	1.85	0.15	0.75
-0.80	-1.30	0.15	0.58
-0.45	-3.65	0.15	0.75
-0.30	-3.50	0.11	0.58
-1.20	-3.55	0.15	0.75
-1.30	-2.75	0.15	0.75
0.55	1.35	0.15	0.72
0.10	-1.00	0.15	0.47
0.60	1.10	0.12	0.66
0.05	1.05	0.15	0.60
-0.05	-0.30	0.15	0.30
0.40	1.65	0.15	0.75
0.10	-0.85	0.15	0.75
0.75	1.30	0.15	0.75
0.40	1.30	0.15	0.75
0.10	-0.15	0.15	0.64
-1.20	-0.55	0.15	0.61
-0.80	-0.90	0.15	0.75
-0.60	0.70	0.15	0.75
-1.00	-1.25	0.15	0.65
-0.00	-0.00	0.15	0.39
-0.00	-0.00	0.15	0.22
0.15	-0.75	0.15	0.55
0.80	-0.10	0.15	0.45
0.30	-0.00	0.15	0.41
0.75	1.35	0.15	0.49
-0.00	0.10	0.15	0.50
-0.00	-0.85	0.15	0.40
-0.00	-0.45	0.15	0.52
-0.00	0.15	0.15	0.38
-0.25	-0.85	0.15	0.75
-0.30	-1.10	0.15	0.75
0.05	2.40	0.15	0.75
-0.05	-0.95	0.08	0.75
-1.00	-3.20	0.15	0.75
-0.20	-0.50	0.15	0.75
-0.30	-2.30	0.15	0.75
-0.25	-2.10	0.15	0.75
0.15	-0.80	0.15	0.75
0.15	-1.40	0.15	0.68
-0.45	-1.95	0.15	0.75

-0.05	-0.50	0.15	0.59
-0.25	-4.60	0.15	0.75
0.30	0.25	0.15	0.75
0.10	-1.75	0.15	0.75
0.60	-0.40	0.15	0.75
0.05	-0.15	0.15	0.75
0.20	-2.05	0.15	0.75
-0.75	-3.95	0.15	0.75
-0.75	-3.45	0.15	0.59
-0.30	-4.90	0.15	0.75
-0.95	-4.25	0.15	0.75
-0.70	-3.55	0.15	0.75
0.50	1.00	0.15	0.75
1.10	2.35	0.15	0.75
0.70	0.85	0.15	0.75
1.40	2.40	0.15	0.75
-0.10	1.35	0.15	0.75
0.50	0.70	0.15	0.75
-0.60	-3.70	0.15	0.75
0.10	-2.95	0.15	0.75
-0.25	-3.85	0.15	0.75
0.25	-2.80	0.15	0.56
-0.30	-3.20	0.15	0.75
-0.30	-4.40	0.15	0.46
-0.40	-3.85	0.15	0.69
-0.55	-3.45	0.15	0.75
-0.10	-2.45	0.15	0.58
0.25	-2.40	0.15	0.71
-0.70	-2.95	0.15	0.75
-0.10	-0.95	0.15	0.75
-0.40	-0.00	0.15	0.75
-0.50	-0.00	0.15	0.75
-0.10	-0.00	0.15	0.75
0.25	-0.00	0.10	0.75
-0.55	-0.00	0.15	0.75
-0.15	-0.00	0.15	0.75
-0.85	-3.90	0.15	0.74
-0.15	-1.70	0.15	0.54
-0.40	-3.85	0.15	0.54
-0.25	-3.50	0.13	0.75
-0.40	-2.15	0.15	0.61
-0.60	-3.75	0.15	0.47
-1.20	-3.95	0.15	0.75
-0.40	-4.20	0.15	0.75

-0.20	-4.05	0.15	0.75
-0.80	-4.85	0.15	0.75
-0.40	-0.35	0.15	0.73
0.15	-0.05	0.15	0.63
-0.80	-3.40	0.15	0.75
-1.20	-4.25	0.15	0.75
-0.55	-2.50	0.15	0.47
-0.45	-3.55	0.15	0.71
-1.20	-3.10	0.15	0.75
-0.40	-2.20	0.15	0.46
-0.25	-2.25	0.15	0.75
0.55	-0.55	0.15	0.75
-0.10	-1.90	0.15	0.75
0.55	-0.50	0.15	0.75
0.50	-0.55	0.15	0.75
-0.15	-1.60	0.15	0.75
-0.25	-2.00	0.15	0.75
0.30	-0.15	0.15	0.75
0.05	-2.95	0.15	0.75
0.55	-0.95	0.11	0.75
0.20	-2.15	0.15	0.75
-0.15	-2.65	0.15	0.75
-0.45	-2.45	0.15	0.75
-0.55	-3.50	0.15	0.75
-0.10	-1.40	0.15	0.75
-0.05	-1.60	0.15	0.75
-0.60	-2.60	0.15	0.75
-0.20	-0.70	0.15	0.75
0.50	0.25	0.15	0.75
1.15	1.60	0.15	0.75
0.35	0.85	0.15	0.75
-0.70	-3.90	0.15	0.71
-1.15	-4.65	0.15	0.75
-0.45	-2.90	0.15	0.68
-0.45	-4.50	0.15	0.75
-0.45	-2.85	0.15	0.74
-0.75	-1.55	0.15	0.75
-0.05	-1.90	0.15	0.75
-0.05	0.65	0.15	0.75
0.60	0.75	0.15	0.75
0.55	-2.00	0.15	0.75
0.65	-1.05	0.15	0.75
0.40	-2.10	0.15	0.75
-0.00	-1.10	0.15	0.75

-0.00	-0.05	0.15	0.75
-0.00	-1.90	0.15	0.44
-0.00	0.65	0.15	0.75
-0.00	-0.45	0.15	0.48
-2.00	-3.20	0.15	0.75
-1.70	-3.35	0.15	0.54
-1.60	-2.40	0.15	0.46
-1.45	-2.85	0.15	0.62
-1.90	-2.90	0.15	0.75
-1.45	-1.80	0.15	0.48
0.40	2.10	0.15	0.75
0.15	-0.70	0.15	0.75
0.25	-0.70	0.15	0.75
0.30	1.50	0.15	0.75
0.10	-1.50	0.15	0.75
-0.20	0.10	0.15	0.53
0.05	-0.20	0.15	0.49
0.60	-1.95	0.15	0.25
-0.25	-0.15	0.15	0.39
0.30	-0.00	0.15	0.44
-0.00	-2.90	0.15	0.75
0.25	-1.80	0.15	0.75
-0.45	-3.50	0.15	0.60
-0.00	0.50	0.15	0.43
-0.30	-0.35	0.12	0.65
0.25	1.05	0.15	0.50
-0.15	-0.75	0.15	0.43
0.70	1.35	0.15	0.72
-0.00	-0.20	0.15	0.63
-0.20	0.45	0.14	0.33
-0.10	-1.25	0.15	0.75
0.30	-0.30	0.15	0.75
-0.00	-2.00	0.15	0.54
0.70	-0.25	0.15	0.75
0.25	-0.85	0.15	0.75
-0.10	-1.20	0.15	0.50
-0.05	-0.75	0.15	0.75
-0.15	-1.75	0.15	0.75
0.20	0.40	0.15	0.75
0.55	-0.00	0.15	0.75
-0.25	-1.50	0.15	0.75
0.40	1.20	0.15	0.75
-0.30	-1.65	0.15	0.43
-0.40	-2.35	0.15	0.75

0.10	-1.25	0.15	0.44
0.10	-2.95	0.15	0.64
-0.40	-2.25	0.15	0.56
-0.15	-1.10	0.15	0.39
-0.45	-0.70	0.15	0.58
-0.65	0.15	0.15	0.34
0.05	0.80	0.15	0.33
-0.00	-0.75	0.15	0.66
-0.60	-0.55	0.15	0.54
-0.00	0.25	0.15	0.73
-0.55	0.75	0.15	0.68
-0.30	-1.80	0.15	0.75
-0.75	-3.05	0.15	0.75
-0.05	-0.75	0.15	0.59
-0.05	-2.25	0.15	0.75
-0.55	-1.95	0.15	0.75
-0.20	-1.10	0.15	0.72
0.35	-0.65	0.15	0.75
0.35	-1.20	0.15	0.75
-0.30	-2.10	0.15	0.75
0.45	-0.20	0.15	0.75
0.50	0.75	0.15	0.75
-0.10	-4.10	0.13	0.75
-0.35	-4.55	0.11	0.75
0.25	-2.10	0.09	0.75
0.55	-2.50	0.09	0.75
-0.60	-4.40	0.11	0.75
0.30	-2.30	0.09	0.75
-0.40	-1.25	0.15	0.55
0.25	-0.10	0.15	0.68
-0.15	-1.80	0.15	0.68
0.50	-0.00	0.13	0.37
0.05	-0.70	0.15	0.70
-0.20	-1.30	0.15	0.75
-0.50	-3.75	0.15	0.75
-0.00	-3.30	0.15	0.64
0.30	-2.55	0.15	0.75
-0.10	-3.65	0.15	0.65
-0.30	-4.95	0.15	0.69
-1.10	-2.85	0.15	0.75
-0.60	-3.05	0.15	0.75
-0.05	-4.00	0.15	0.75
-0.85	-2.50	0.15	0.75
-0.20	-2.05	0.15	0.68

0.75	0.30	0.15	0.75
-0.50	0.35	0.15	0.75
-0.80	0.20	0.15	0.75
-0.10	0.80	0.15	0.75
-0.05	0.25	0.13	0.75
-0.80	0.40	0.15	0.75
-0.15	1.10	0.15	0.75
-0.05	-0.70	0.15	0.44
-0.25	-0.65	0.15	0.56
0.40	0.30	0.15	0.36
0.30	-1.20	0.15	0.67
-0.40	-0.50	0.15	0.41
0.25	0.30	0.15	0.61
0.10	0.05	0.15	0.58
0.35	1.00	0.15	0.75
0.05	0.15	0.15	0.75
0.75	1.05	0.15	0.60
0.55	0.55	0.15	0.69
-0.70	-1.20	0.15	0.67
-0.30	0.35	0.15	0.47
-0.25	-0.20	0.15	0.48
0.25	0.60	0.12	0.75
-0.30	0.35	0.15	0.56
-0.15	-2.65	0.15	0.75
0.05	-2.40	0.15	0.49
-0.05	-3.70	0.15	0.65
-0.80	-3.10	0.15	0.75
0.40	-2.30	0.15	0.52
A2			
-0.55	-3.65	0.15	0.71
-0.80	-3.75	0.15	0.39
-0.60	-3.65	0.15	0.43
-0.60	-3.50	0.15	0.31
-0.40	-2.45	0.15	0.39
-0.85	-3.80	0.15	0.41
-0.60	-2.75	0.15	0.23
-0.75	-3.15	0.15	0.60
-0.85	-2.90	0.15	0.21
0.20	-0.05	0.12	0.28
-0.10	-0.15	0.15	0.21
0.05	0.30	0.12	0.29
0.15	0.65	0.11	0.26
0.05	-0.05	0.12	0.28
-0.00	-0.05	0.13	0.27

-0.20	-0.95	0.14	0.43
0.25	0.05	0.15	0.75
0.15	-0.45	0.15	0.46
-0.20	-0.50	0.15	0.75
0.30	1.50	0.15	0.75
-0.45	-0.55	0.15	0.62
-0.05	-0.15	0.15	0.75
-0.15	-2.05	0.15	0.64
-0.15	-2.30	0.12	0.34
-0.30	-2.50	0.13	0.49
-0.15	-1.65	0.15	0.67
-0.15	-1.00	0.10	0.46
0.05	-1.85	0.12	0.37
-0.45	-2.25	0.12	0.75
0.25	-1.40	0.13	0.53
-0.40	-2.05	0.15	0.75
-0.10	-1.55	0.15	0.75
-0.30	-0.80	0.15	0.61
-0.35	-2.35	0.15	0.75
-0.50	-2.70	0.14	0.75
-0.05	-2.00	0.15	0.75
-0.15	-1.90	0.15	0.75
-0.00	-1.75	0.15	0.75
0.20	-1.00	0.15	0.75
0.40	0.20	0.15	0.75
0.05	-2.20	0.15	0.75
-0.00	-2.70	0.14	0.75
-0.00	-2.10	0.15	0.75
0.55	-1.25	0.13	0.75
-0.05	-2.35	0.13	0.75
0.10	0.25	0.09	0.44
-0.05	-0.95	0.15	0.56
-0.00	-0.40	0.15	0.42
0.70	-0.05	0.13	0.38
-0.55	-2.05	0.15	0.70
-0.55	-1.70	0.15	0.42
-0.80	-2.00	0.15	0.49
-0.55	-1.75	0.15	0.49
-0.45	-1.70	0.13	0.62
-0.30	-1.00	0.14	0.45
-0.45	-1.70	0.15	0.68
-0.65	-1.55	0.10	0.50
-0.65	-1.10	0.15	0.75
-0.75	-0.90	0.15	0.75

-0.10	0.05	0.15	0.52
-0.10	-0.35	0.15	0.71
-0.20	0.05	0.15	0.47
-0.10	-0.30	0.15	0.75
0.10	-1.05	0.07	0.40
-0.15	-2.20	0.12	0.26
0.10	-2.05	0.11	0.53
-0.00	-2.10	0.09	0.45
-0.00	-2.00	0.09	0.34
-0.10	-2.15	0.13	0.32
0.35	-0.65	0.08	0.37
-0.10	-1.40	0.15	0.40
-0.00	-0.95	0.09	0.26
0.10	-0.95	0.11	0.29
-0.35	0.05	0.14	0.33
-0.50	-1.30	0.14	0.35
0.05	-0.10	0.09	0.30
-0.05	-0.05	0.09	0.47
-0.00	0.15	0.09	0.29
0.10	0.40	0.13	0.32
0.25	0.65	0.11	0.28
-0.10	-0.25	0.09	0.27
-0.10	-0.10	0.08	0.28
-0.20	-0.60	0.12	0.34
-0.00	-0.30	0.13	0.31
0.20	0.40	0.09	0.33
-0.05	0.40	0.15	0.31
0.25	1.35	0.11	0.56
-0.20	0.25	0.13	0.32
-0.35	-0.00	0.15	0.75
-0.60	-0.00	0.14	0.75
-0.10	-0.00	0.11	0.75
-0.05	-0.00	0.07	0.75
-0.00	-0.00	0.11	0.75
0.15	-0.00	0.06	0.75
-0.20	-0.00	0.08	0.75
-0.20	-0.00	0.09	0.75
-0.00	-0.00	0.12	0.75
0.15	-0.00	0.09	0.75
-0.10	-0.00	0.11	0.75
0.15	-0.00	0.09	0.75
-0.40	-0.00	0.13	0.75
-0.10	0.35	0.08	0.60
-0.45	-2.10	0.10	0.73

-0.25	-1.40	0.13	0.63
-0.30	-0.40	0.10	0.51
-0.20	-0.45	0.08	0.61
-0.10	-1.05	0.07	0.58
-0.25	-1.50	0.11	0.51
-0.40	-1.60	0.11	0.45
-0.35	-1.45	0.12	0.55
-0.50	-1.05	0.11	0.70
-0.20	-0.80	0.15	0.69
-0.60	-1.55	0.15	0.48
-0.45	-1.00	0.14	0.72
-0.30	-0.10	0.12	0.63
-0.50	-2.15	0.12	0.49
-0.80	-2.80	0.11	0.39
-0.50	-1.65	0.08	0.48
-0.70	-1.45	0.11	0.44
-0.50	-1.35	0.14	0.56
-0.55	-1.80	0.11	0.64
-0.55	-1.85	0.11	0.26
-0.65	-2.10	0.14	0.29
-0.15	-1.15	0.07	0.29
-0.70	-2.45	0.14	0.26
-0.40	-1.50	0.12	0.26
-0.20	-1.95	0.07	0.29
-0.45	-2.65	0.14	0.75
-0.15	-1.45	0.11	0.75
-0.25	0.05	0.13	0.75
-0.15	-2.55	0.08	0.75
-0.10	-2.15	0.10	0.75
-0.30	-2.35	0.15	0.75
-0.40	-1.70	0.15	0.66
-0.50	-2.40	0.15	0.75
-0.00	-1.55	0.11	0.75
-0.30	-2.00	0.15	0.72
-0.30	-1.35	0.13	0.58
-0.10	-1.35	0.13	0.75
-0.45	-0.40	0.15	0.36
-0.15	-1.40	0.11	0.34
-0.25	-1.25	0.09	0.25
-0.15	-1.40	0.11	0.32
-0.10	-1.95	0.15	0.51
0.05	-2.05	0.13	0.75
-0.15	-1.65	0.09	0.27
-0.25	-0.90	0.09	0.31

-0.25	0.25	0.15	0.35
-0.20	1.55	0.15	0.48
-0.55	-2.60	0.15	0.45
-0.50	-1.90	0.10	0.69
-0.70	-1.65	0.14	0.43
-0.55	-2.10	0.08	0.65
-0.50	-2.00	0.08	0.75
-0.70	-2.25	0.09	0.75
-0.05	-0.40	0.08	0.49
-0.10	-0.95	0.08	0.55
-0.00	0.60	0.10	0.49
0.05	1.35	0.15	0.75
-0.50	-2.35	0.15	0.75
-0.35	-1.55	0.15	0.75
-0.55	-2.25	0.15	0.59
-0.00	-1.05	0.15	0.45
-0.00	-0.55	0.15	0.63
-0.65	-0.35	0.09	0.47
-0.65	-3.70	0.15	0.75
-0.90	-0.65	0.11	0.75
-0.15	0.55	0.15	0.75
0.10	-0.30	0.10	0.54
-0.20	-0.80	0.12	0.68
0.30	-1.80	0.15	0.73
0.45	0.20	0.15	0.46
-0.80	-3.55	0.13	0.37
-0.55	-2.45	0.09	0.51
-0.75	-2.30	0.11	0.51
-0.55	-2.20	0.08	0.37
-0.50	-1.95	0.09	0.40
-0.30	-1.40	0.09	0.45
-0.55	-2.55	0.09	0.37
-0.70	-2.50	0.10	0.45
-0.70	-2.00	0.10	0.45
-0.80	-2.10	0.14	0.56
-0.15	-0.70	0.08	0.46
-0.35	-1.25	0.10	0.62
-0.40	-0.65	0.10	0.68
-0.20	-1.55	0.14	0.66
-0.55	-0.10	0.15	0.39
-0.15	-0.30	0.09	0.31
-0.25	0.20	0.10	0.39
-0.15	0.45	0.10	0.62
-0.10	0.55	0.08	0.57

-0.10	0.85	0.09	0.53
-0.20	-0.15	0.13	0.27
-0.20	0.25	0.10	0.51
-0.10	0.50	0.10	0.36
0.20	1.30	0.15	0.65
0.40	2.05	0.15	0.49
0.05	2.15	0.08	0.57
0.30	2.00	0.13	0.62
-0.00	2.35	0.11	0.57
A3			
0.20	-1.35	0.15	0.75
0.25	0.70	0.13	0.75
-0.65	-2.40	0.15	0.61
0.60	0.80	0.15	0.29
0.35	-0.30	0.15	0.32
0.25	-1.30	0.15	0.32
0.50	0.05	0.15	0.75
0.20	-1.70	0.12	0.75
-0.70	-1.05	0.15	0.75
-1.75	-2.55	0.15	0.75
-0.40	-2.00	0.13	0.59
-0.05	-2.45	0.15	0.54
-0.05	-2.05	0.15	0.75
0.10	-3.25	0.15	0.75
-0.50	-2.50	0.15	0.75
0.20	0.45	0.15	0.59
0.90	2.10	0.15	0.57
0.05	0.35	0.15	0.61
0.75	1.25	0.15	0.57
0.30	0.75	0.15	0.75
-0.55	-2.00	0.15	0.33
-0.70	-2.90	0.15	0.75
-1.15	-3.95	0.15	0.40
-0.45	-2.90	0.15	0.75
-1.05	-4.10	0.15	0.75
-0.20	-2.40	0.15	0.75
-0.45	-3.75	0.15	0.74
-0.55	-1.50	0.14	0.50
1.10	2.25	0.15	0.70
0.05	-0.15	0.13	0.75
-0.05	0.10	0.15	0.64
0.45	1.25	0.15	0.63
0.80	1.95	0.12	0.75
0.15	0.10	0.14	0.57

0.10	0.65	0.15	0.75
-0.75	-2.75	0.15	0.61
1.00	1.20	0.13	0.75
0.25	-1.10	0.15	0.61
0.55	1.30	0.15	0.75
0.35	0.80	0.14	0.75
0.10	-1.20	0.10	0.75
0.05	-0.15	0.13	0.75
-1.10	-1.35	0.13	0.43
1.00	2.05	0.15	0.75
0.05	0.10	0.13	0.75
0.70	2.05	0.15	0.75
-0.05	0.20	0.15	0.75
0.90	2.25	0.14	0.73
0.20	0.05	0.15	0.75
-0.85	-2.70	0.15	0.74
0.20	0.20	0.15	0.56
0.60	2.05	0.15	0.45
0.20	0.30	0.13	0.75
0.90	2.00	0.15	0.43
-0.75	-0.15	0.15	0.75
-0.65	0.20	0.15	0.75
-1.25	-1.85	0.15	0.57
-1.05	-2.30	0.15	0.35
-1.05	-1.80	0.15	0.32
0.60	0.40	0.15	0.61
0.90	0.40	0.15	0.66
0.95	-0.90	0.15	0.75
0.60	-0.90	0.09	0.64
0.45	1.10	0.15	0.75
0.70	0.70	0.15	0.75
1.05	2.20	0.15	0.75
0.40	0.40	0.11	0.75
0.30	0.10	0.15	0.66
0.40	-0.05	0.15	0.18
0.85	0.90	0.15	0.41
0.95	1.80	0.15	0.22
0.45	-0.40	0.15	0.28
0.40	0.45	0.15	0.26
-1.05	0.30	0.15	0.75
-0.85	-3.00	0.15	0.53
-0.15	-2.35	0.15	0.75
-0.10	-2.10	0.15	0.75
-0.45	-2.25	0.15	0.75

-0.25	-2.80	0.15	0.75
-0.30	-0.75	0.15	0.60
0.90	1.60	0.15	0.75
1.10	2.65	0.15	0.75
0.40	-0.10	0.15	0.75
0.45	-0.15	0.15	0.75
-0.55	-1.95	0.14	0.54
0.30	0.25	0.11	0.75
0.90	2.20	0.15	0.75
1.05	2.35	0.15	0.60
0.35	0.05	0.15	0.75
0.45	0.95	0.15	0.75
-0.60	-2.30	0.08	0.59
-1.20	-3.20	0.13	0.42
-0.60	-1.35	0.15	0.75
-0.10	-1.80	0.15	0.75
-1.05	-3.80	0.15	0.49
-1.15	-2.75	0.15	0.39
-0.60	-0.25	0.11	0.43
0.05	2.10	0.15	0.75
0.20	0.15	0.15	0.75
-1.05	-0.95	0.11	0.57
-0.25	-3.40	0.15	0.75
-0.20	-2.75	0.15	0.75
-0.65	-3.35	0.15	0.75
0.70	1.00	0.15	0.75
0.95	0.85	0.15	0.75
1.20	1.40	0.15	0.75
0.70	0.25	0.15	0.75
0.65	0.45	0.15	0.75
-0.50	-2.45	0.15	0.75
2.15	2.15	0.15	0.75

Table S2. *P*- and *S*-wave relative arrival-time residuals for common earthquake-station pairs for regions *A1, A2* and *A3*. We used these residuals to build Figure 6.

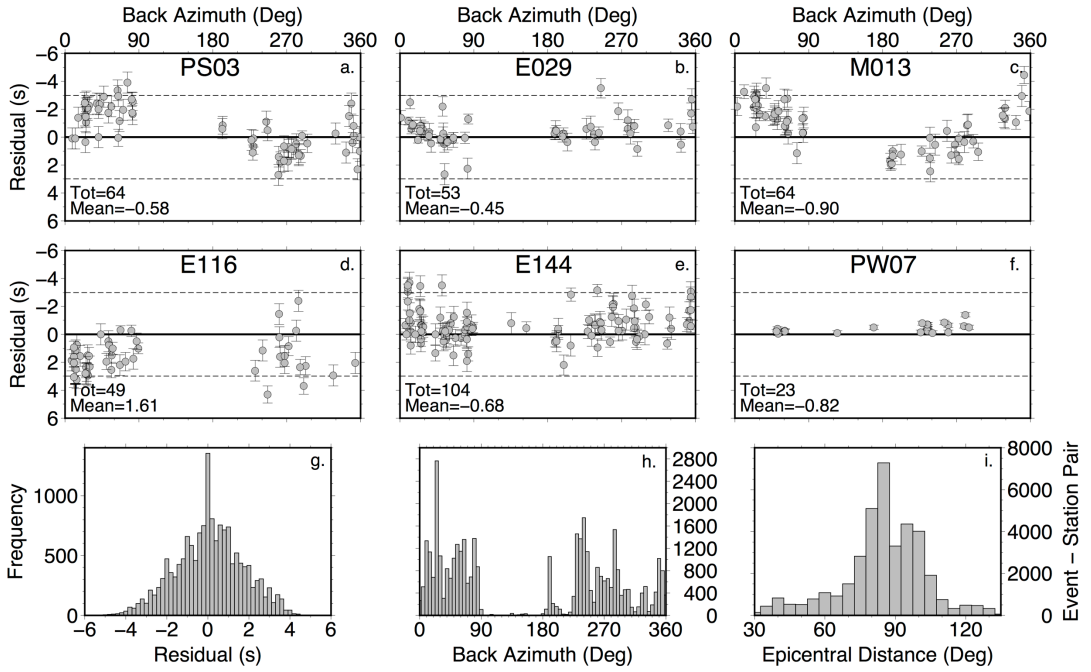

Figure S1. (a, b, c, d, e, f) Distribution of relative arrival-time residuals with error bars as a function of back-azimuth for the six stations labelled in Figure 1. (a) Stations near the Strait of Gibraltar (e.g. PS013) display a general trend of negative residuals (early arrivals, faster velocities) for rays coming in from the *NE* and positive residuals (late arrivals, slower velocities) for rays coming in from the *N* and *S-SW*. This pattern suggests that rays arriving from the *NE* travel through a high-velocity body below the Alboran Sea. On the other hand, waves arriving from the *N*, *S* and *SW* cross predominantly slow structures. (b) Northwards (e.g., E029), some few slightly positive residuals from the *NE* may reflect the low-velocity structure beneath eastern Betics, the Iberian Chain and the Valencia Trough, while negative residuals from the *SE* and *W* result from a high-velocity structure below the Alboran Sea and Western Iberia. (c) Near the northern Moroccan margin (e.g. M013), negative residuals from the *N* and *NW* are largely due to the fast structure beneath the Alboran Sea, while positive residuals are observed for rays coming from the *SW*. (d) Stations deployed in the south of the Pyreenes (e.g. E116) reveal residuals that are mainly positive for rays coming from all directions. This means that rays travel through surrounding low-velocity structures. (e) In spite of a high level of scatter, many residuals in the Cantabrian Mountains (e.g., E144) for rays coming in from the *NE* are positive, suggesting low-velocity anomalies in Central Europe. The negative residuals for rays coming in from the west result from fast material beneath Western Iberia. (f) Residuals in Western Iberia (Portugal, e.g. PW07) generally sample fast structure. (g) Frequency distribution of residuals for the *S*-wave data set. (h) Event frequency with back azimuth. (f) Histogram of epicentral distances.

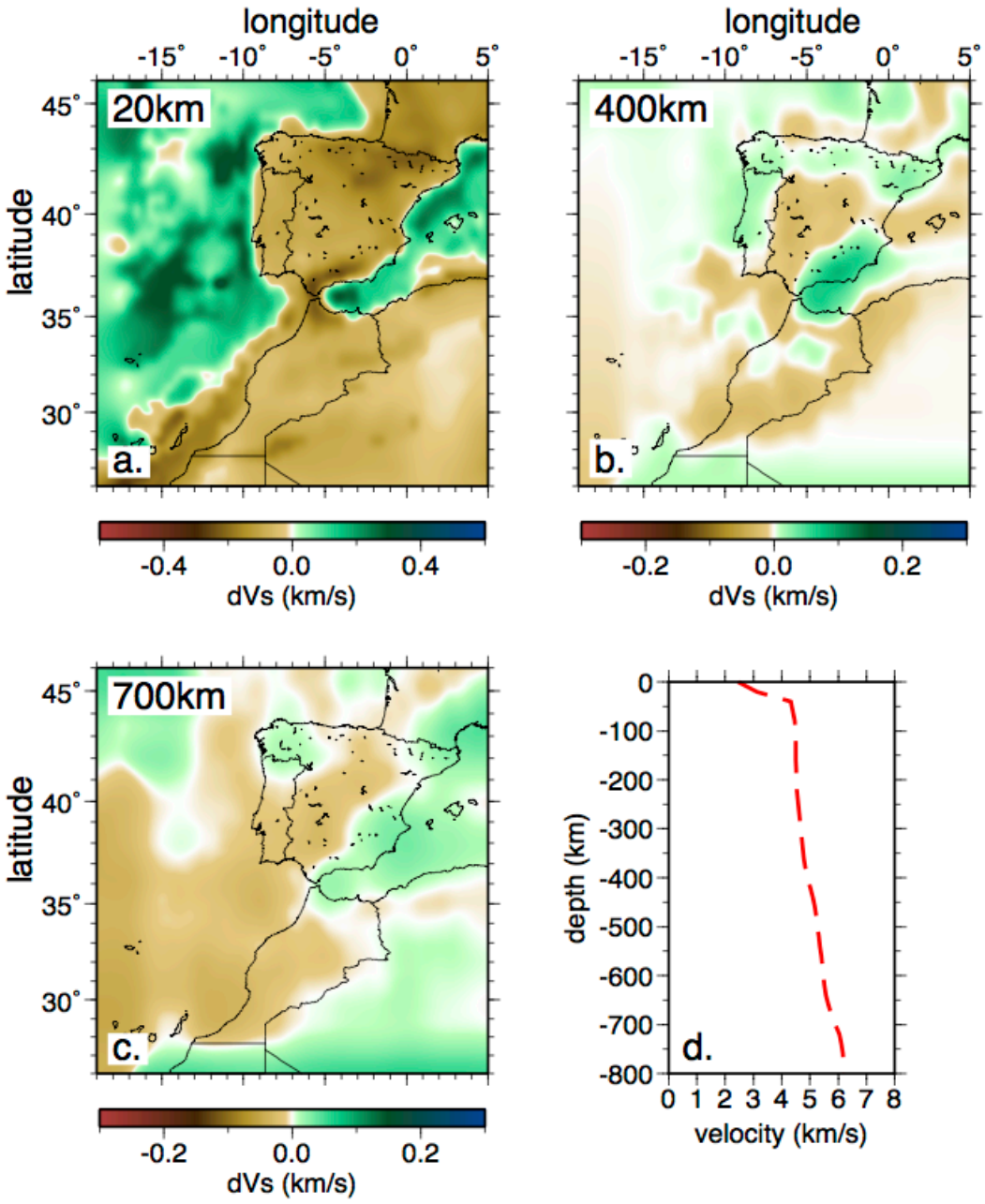

Figure S2. Depth slices through the starting model used for our tomographic inversion. The *S*-wave starting model is obtained from the *P*-wave *PRISM3D* model down to the bottom of the transition zone (660 km depth) and then from *LLNL* for the topmost lower mantle (660-800 km depth), by applying a V_P/V_S ratio calculated from the *1D ak135 P*- and *S*-wavespeed models as a function of depth. (a) 20 km depth slice; (b) 400 km depth slice; (c) 700 km depth slice. (d) *1D* laterally averaged depth-dependent version of the *3D* starting model, used as a reference model for plotting the starting model and our final *S*-wave model.

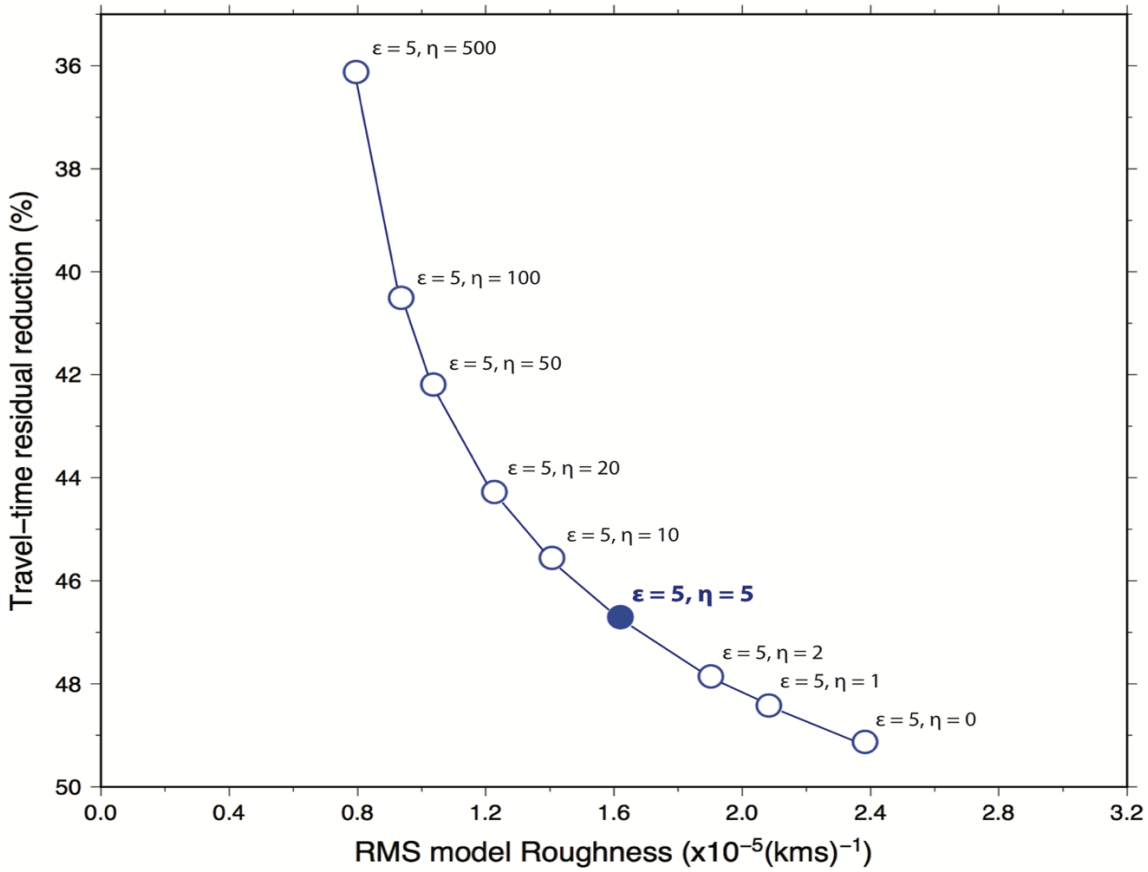

Figure S3. Trade-off between model roughness and data fit for inversions with different degrees of smoothing η while holding the damping parameter ε fixed at the value of 5 (blue circles). This graph represents the last step of the scheme proposed by Rawlinson et al., (2006) to estimate optimum damping and smoothing parameters. Filled circle show final damping and smoothing (ε = 5, η = 5) parameters used for our preferred model.

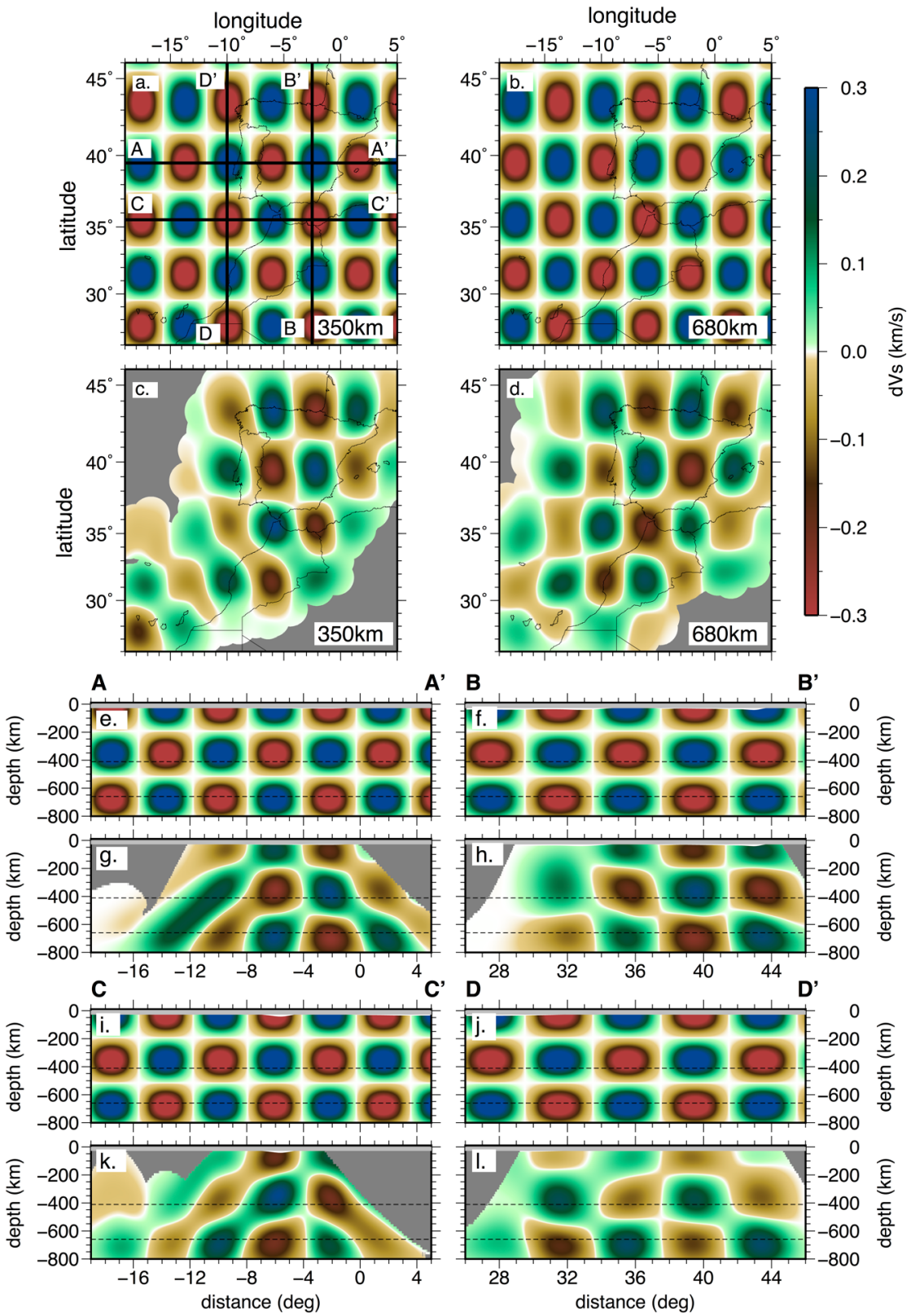

Figure S4. Checkerboard resolution tests for our tomographic study, using an alternating pattern of high- and low-velocity anomalies of ~300-km width and ±0.5 km/s in amplitude separated by a

narrow region of zero perturbation. In this case, velocity perturbations are plotted relative to the *3D* starting model. a, b) Input model at 350 km and 680 km depth respectively. c, d) Output *S*-velocity structure at 350 km and 680 km depth respectively. The raypaths and inversion parameters used are the same as for the inversion of the actual data. Gaussian noise of 0.4 s is added to the synthetic dataset to mimic that in the data. Crustal structure is light grey-shaded. Regions with no piercing points are shaded darker grey. Black lines show coastlines. (e, f, i, j) show vertical cross-sections oriented east-west (e,i) and south-north (f, j), through the input model (the orientations of the profiles are shown in depth slice a.). (g, h, k, l) show vertical cross-sections through the recovered model. Resolution is good down to the base of the model (800 km depth) in Iberia and north-western Morocco, with smearing along rays at the edges of the region, especially beneath the oceanic domain.

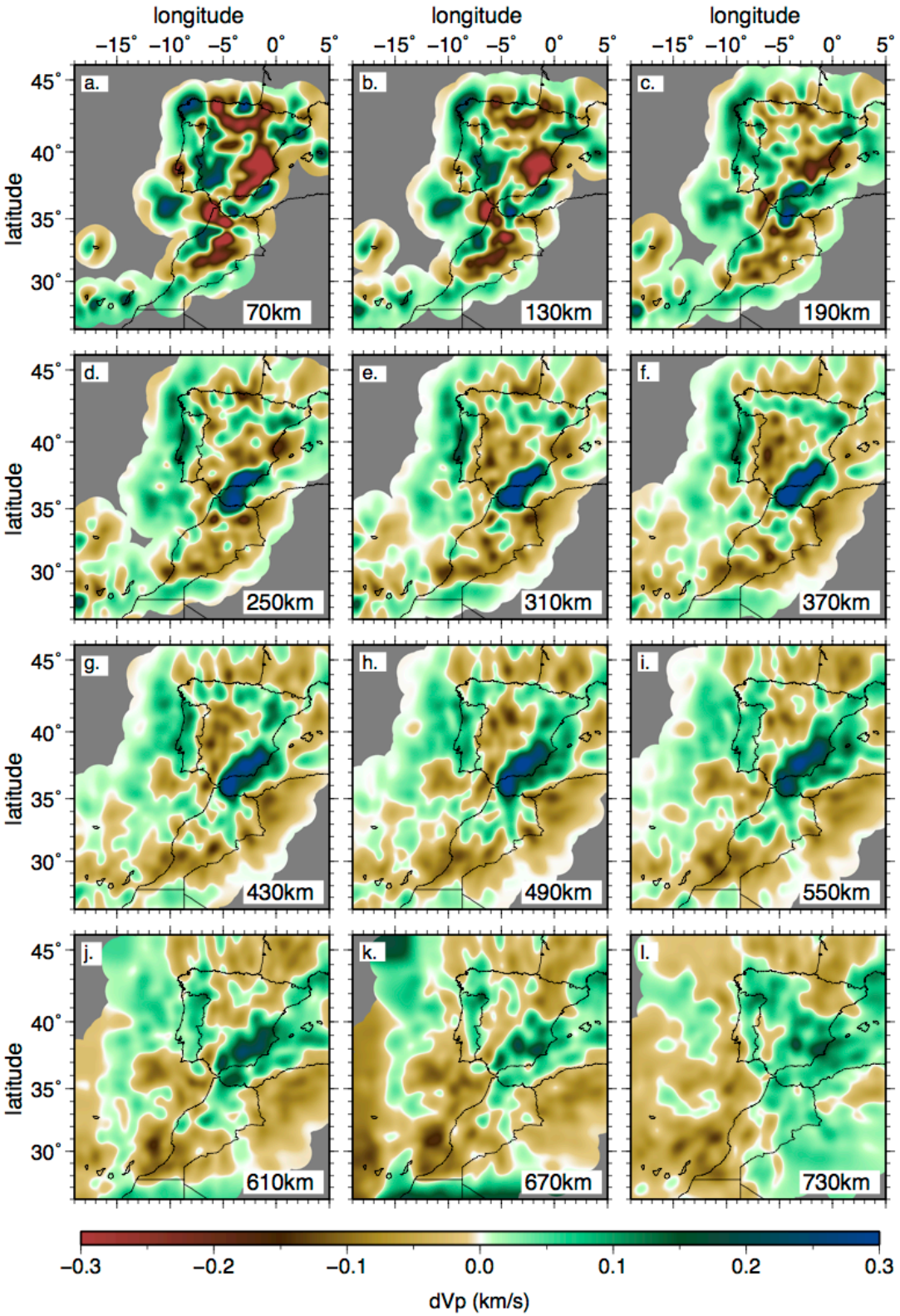

Figure S5. *P*-wave model (*IBEM-P18*) slices ($\varepsilon = 5$, $\eta = 5$) at the depth range 70-730 km taken from Civiero et al., (2018). Regions with no piercing points are shaded grey. Black lines show coastlines. The structures in this model are very similar to those in our *S*-wave model.

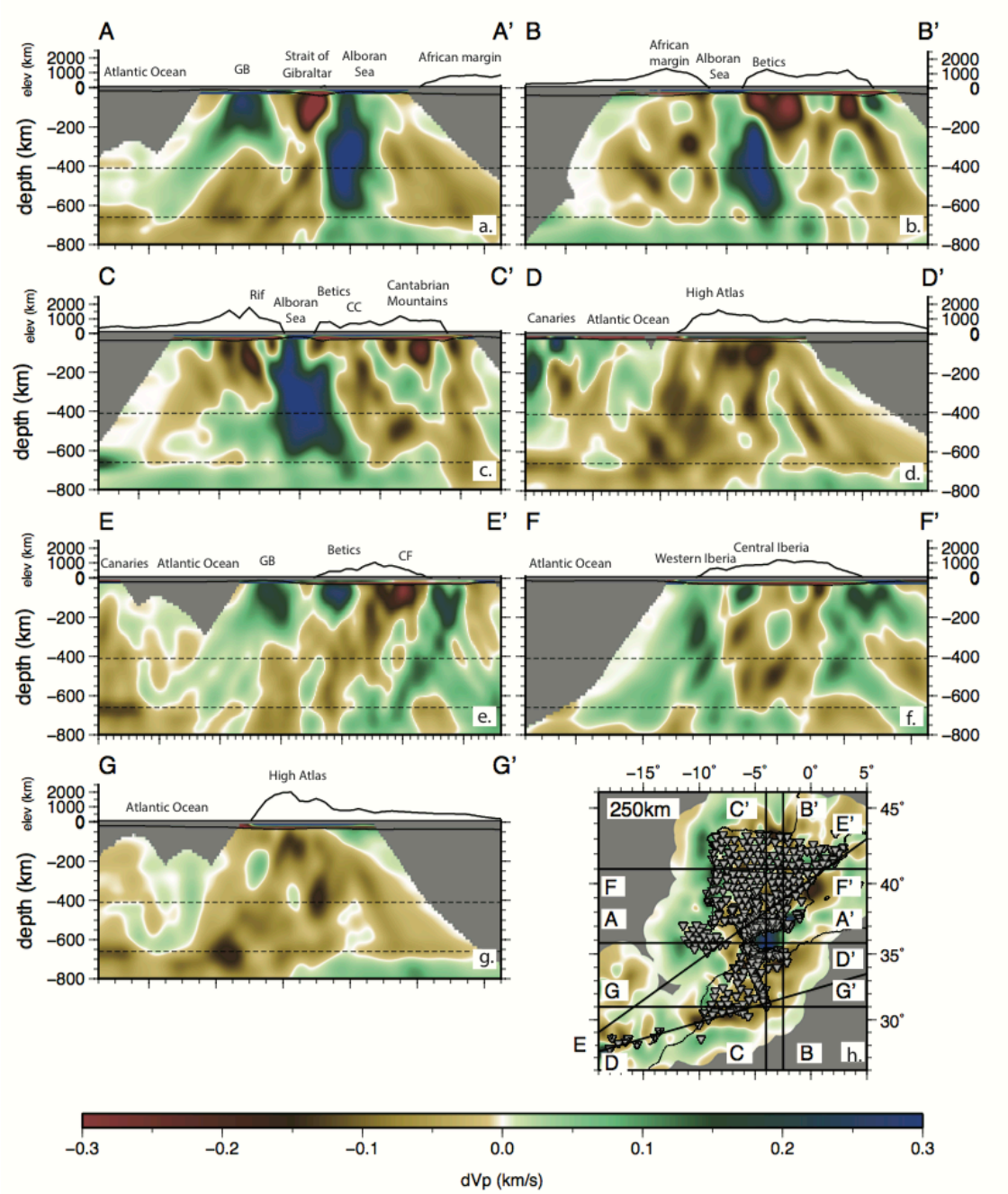

Figure S6. Cross-sections through our *IBEM-P18* ($\varepsilon = 5$, $\eta = 5$). Regions with no piercing points are shaded grey. Black lines show coastlines. Although the spatial resolution is higher in *IBEM-P18* than in the S-wave model, the main low- and high-velocity anomalies discussed and interpreted in our previous work (Civiero et al., 2018) are consistent with those in our *S*-wave model.

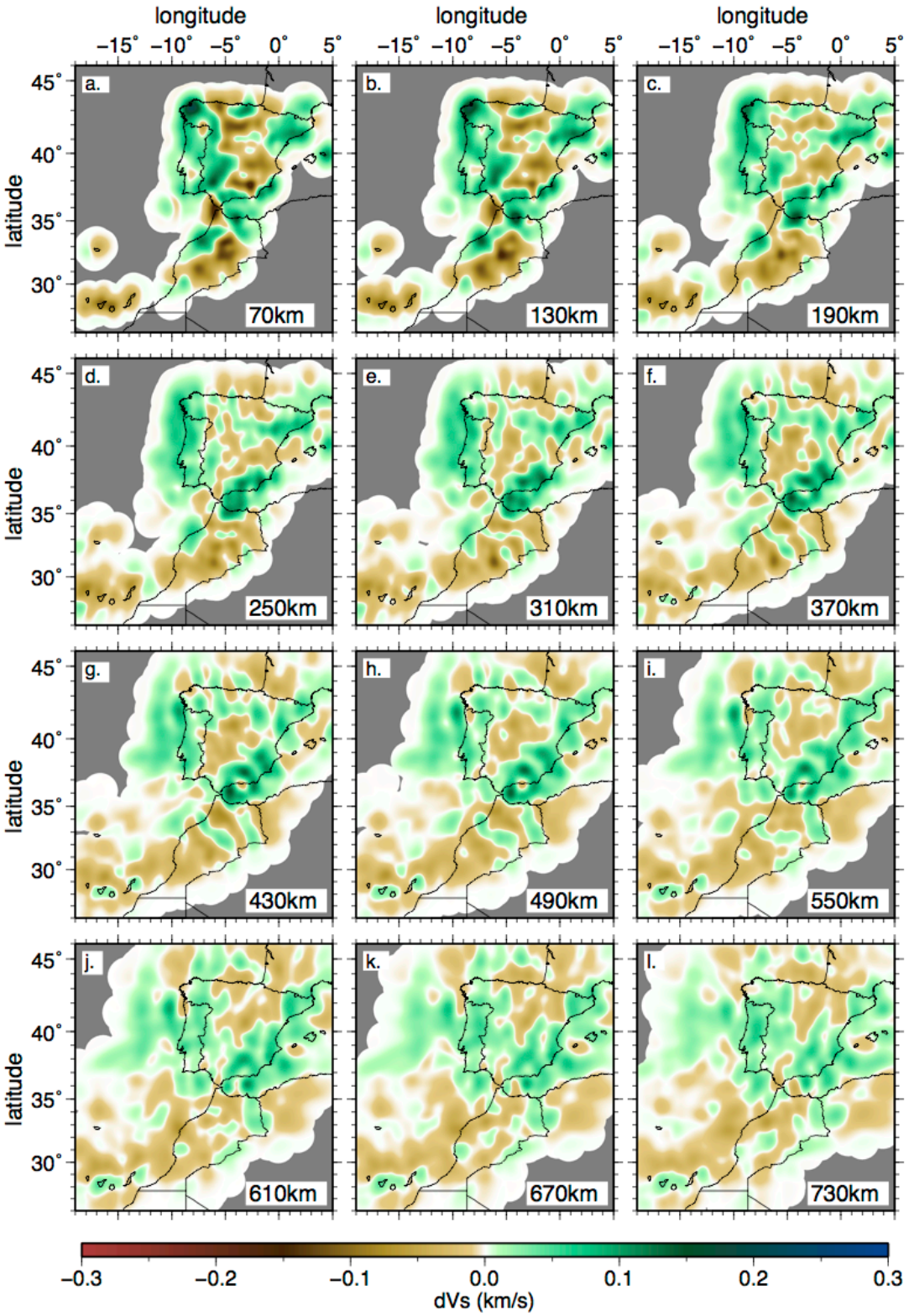

Figure S7. Depth slices through the tomographic *S*-wave model ($\varepsilon = 5$, $\eta = 5$) at a depth range 70-730 km using the *1D* ak135 velocity model (Kennett et al., 1995) as the initial model for the mantle. Regions with no piercing points are shaded grey. Black lines show coastlines. The same low- and high-velocity anomalies are present although the amplitude here is much lower.

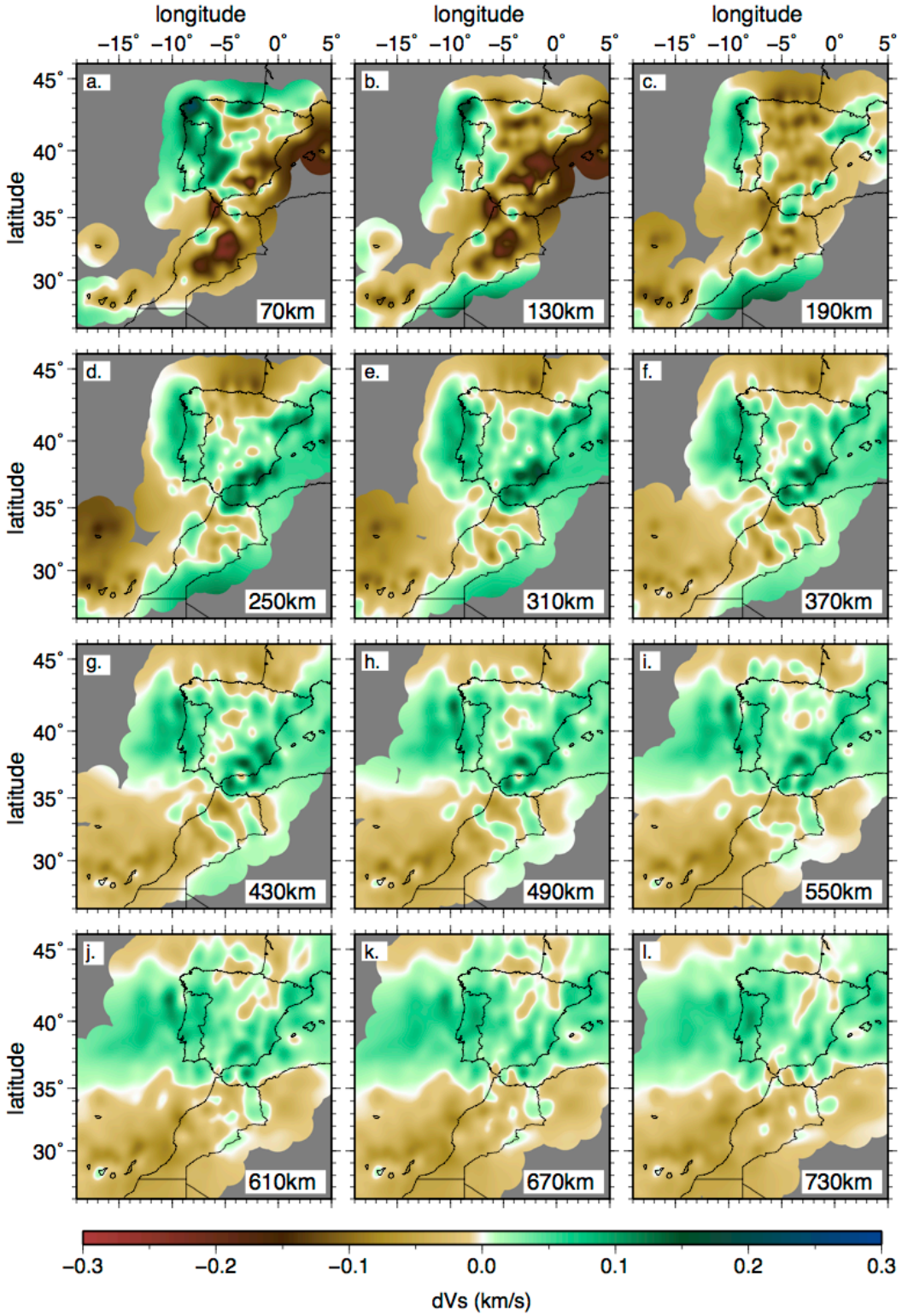

Figure S8. Depth slices through the tomographic *S*-wave model ($\varepsilon = 5$, $\eta = 5$) at a depth range 70-730 km using the independently constrained *SeMum2* velocity model (French et al., 2013) as the initial model for the mantle. Velocities are plotted relative to a *1D* laterally averaged depth-dependent version of *SeMum2*. Regions with no piercing points are shaded grey. Black lines show coastlines. At lithospheric depths the low-velocity features below Canaries, Atlas Ranges and Rif-

Betics System are much stronger than those in our preferred *S*-wave model and in our previous *P*-wave model (Civiero et al., 2018) reflecting a possible effect of melting or fluids in the origin of seismic anomalies.

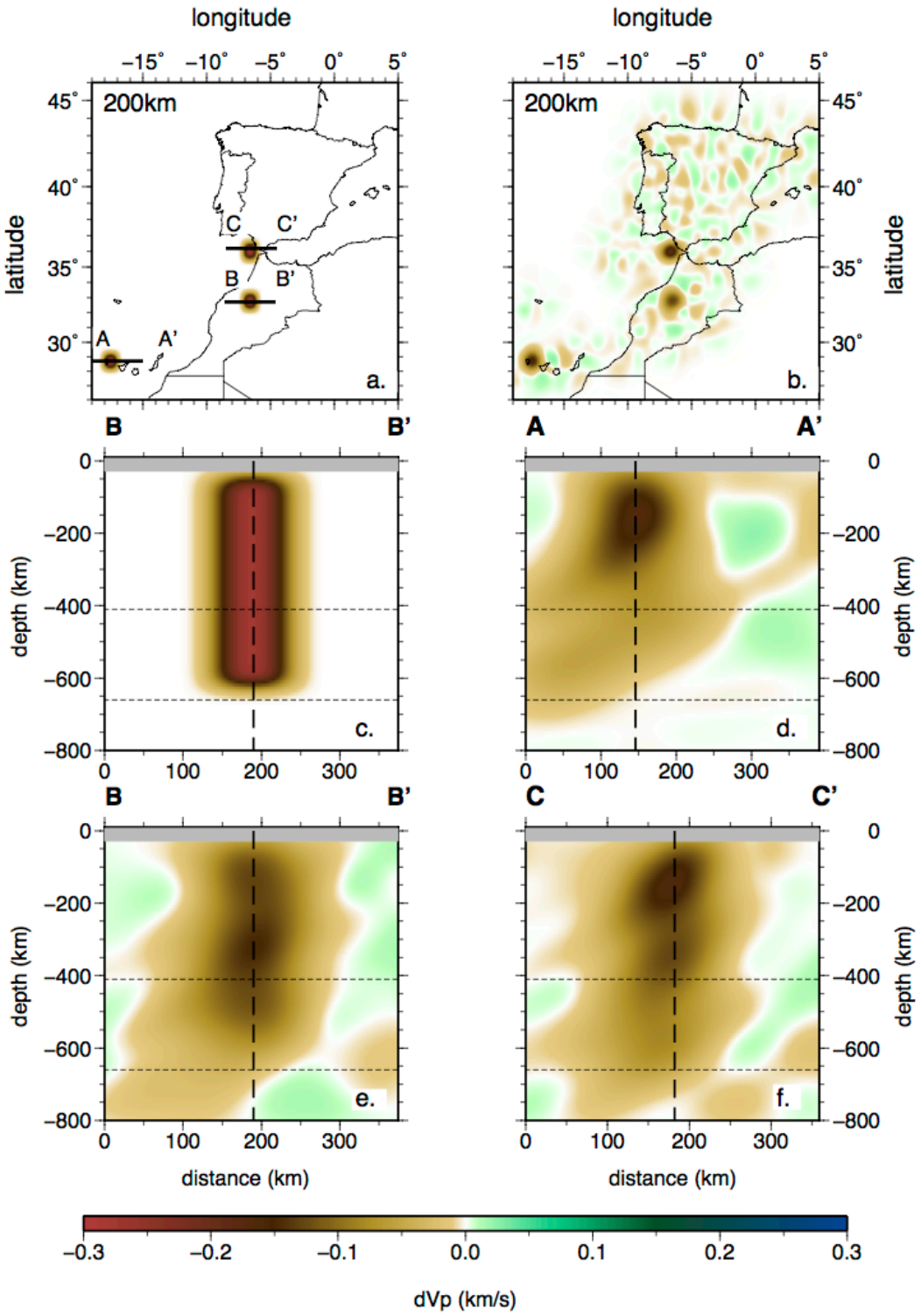

Figure S9. Structural resolution test for the *P*-wave tomographic study (Civiero et al., 2018), using synthetic vertical low-velocity structures below the Canaries, the Atlas Ranges and the Gibraltar Arc (-0.3 km/s amplitude). Velocity perturbations are plotted relative to the *3D* starting model. (a) Map view of the input model at 200 km depth. (b) Map view of the recovered model at 200 km depth. (c) Input model through vertical cross-sections oriented west-east below the Canaries (the same input structure is located below the Atlas Ranges and the Gibraltar Arc). The

orientations of the profiles are shown in depth slice a). (d, e, f) Vertical cross-sections through the recovered model. The same raypaths and inversion parameters that are used in the inversion of the observations are used here and Gaussian noise of 0.1 s standard deviation is added to the synthetic dataset to mimic the noise in the observations. Crustal structure is grey-shaded. The amplitude recovery of the vertical bodies is around 50% in their centre ,down to 400-500 km depth for the cases (e) and (f), and down to around 250 km for case (d).

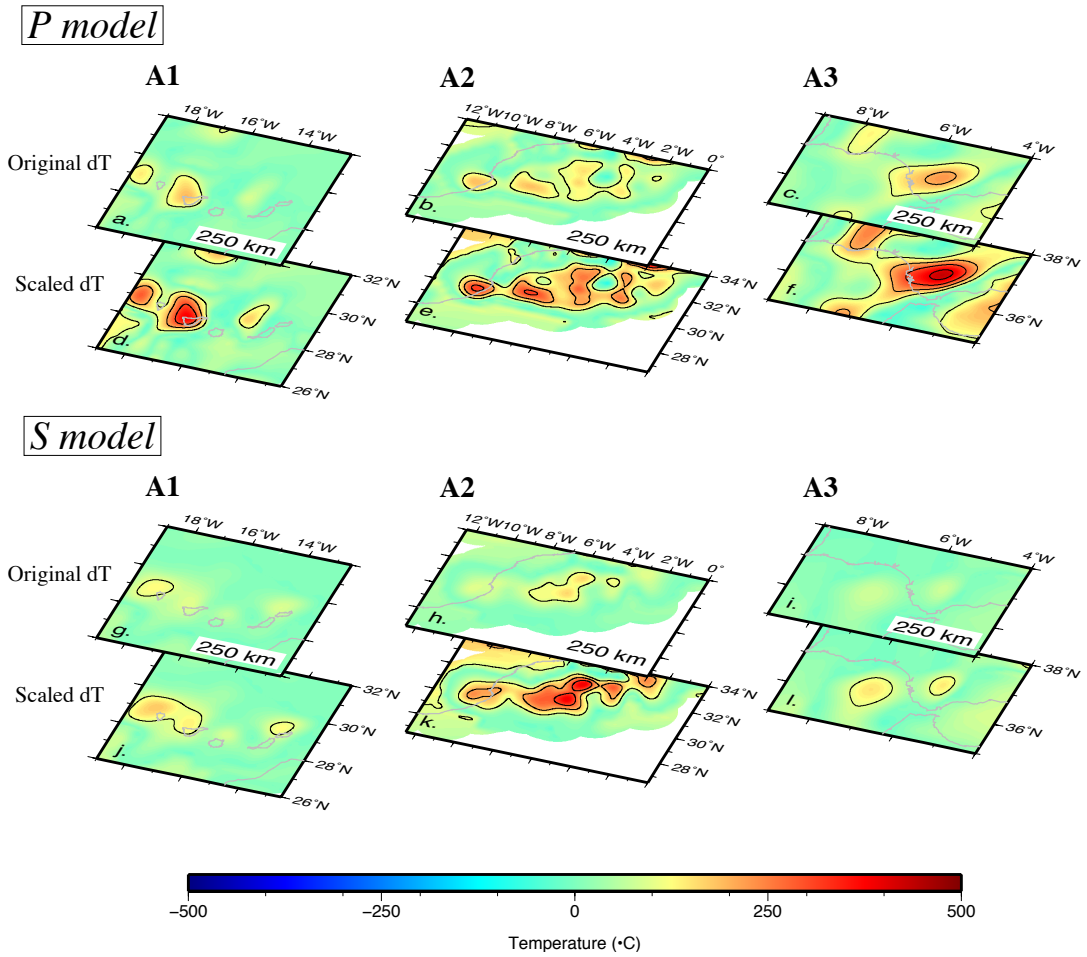

Figure S10. Horizontal slices at 250 km depth showing the thermal anomalies obtained from the conversion of both *P*- and *S*-wave velocities below the imaged upwellings within *A1*, *A2* and *A3*. The maximum low-velocity perturbation in the input synthetic structures is 0.1 km/s. a, b, c) Original *T* excesses derived from the *P*-wave velocities in *IBEM-P18*. d, e, f) Scaled *T* excesses derived from the *P*-wave velocities in *IBEM-P18*. g, h, i) Original *T* excesses derived from the *S*-wave velocities. j, k, l) Scaled *T* excesses derived from the *S*-wave velocities. Regions with no piercing points are shaded white. Grey lines show coastlines. The spacing between the contours is 100°C.

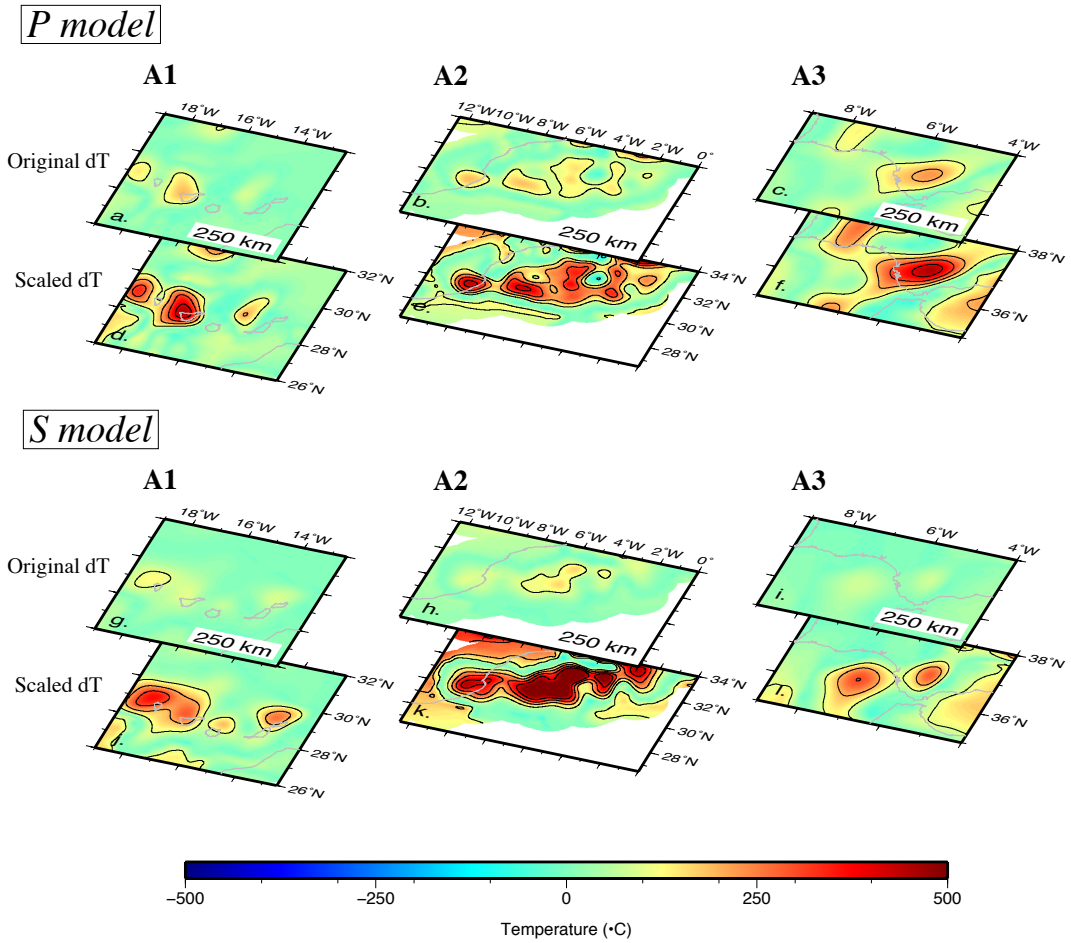

Figure S11. Horizontal slices at 250 km depth showing the thermal anomalies obtained from the conversion of both *P*- and *S*-wave velocities below the imaged upwellings within *A1*, *A2* and *A3*. The maximum low-velocity perturbation in the input synthetic structures is 0.6 km/s. a, b, c) Original *T* excesses derived from the *P*-wave velocities in *IBEM-P18*. d, e, f) Scaled *T* excesses derived from the *P*-wave velocities in *IBEM-P18*. g, h, i) Original *T* excesses derived from the *S*-wave velocities. j, k, l) Scaled *T* excesses derived from the *S*-wave velocities. Regions with no piercing points are shaded white. Grey lines show coastlines. The spacing between the contours is 100°C.

References:

Civiero, C., Strak, V., Custódio, S., Silveira, G., Rawlinson, N., Arroucau, P., & Corela, C. (2018). A common deep source for upper-mantle upwellings below the Ibero-western Maghreb region from teleseismic P -wave travel-time tomography. *Earth and Planetary Science Letters*, *499*, 157–172. https://doi.org/10.1016/j.epsl.2018.07.024

French, S. W., Lekić, V., & Romanowicz, B. (2013). Waveform Tomography Reveals Channeled Flow at the Base of the Oceanic Asthenosphere. *Science*, *355*(6359), 437–440. https://doi.org/10.1038/355437a0

Kennett, B. L. N., Engdahl, E. R., & Buland, R. (1995). Constraints on seismic velocities in the Earth from travel times. *Geophysical Journal International*, *122*, 108–124. https://doi.org/10.1111/j.1365-246X.1995.tb03540.x

Rawlinson, N., Reading, A. M., & Kennett, B. L. N. (2006). Lithospheric structure of Tasmania from a novel form of teleseismic tomography. *Journal of Geophysical Research: Solid Earth*, *111*(2), 1–21. https://doi.org/10.1029/2005JB003803